

TF-RESTORMER: COMPLEX SPECTRAL PREDICTION FOR SPEECH RESTORATION

Ui-Hyeop Shin¹, Jaehyun Ko², Woocheol Jeong², Hyung-Min Park^{1,2}

Department of ¹Electronic Engineering, ²Artificial Intelligence

Sogang University, Seoul, Republic of Korea,

{dmlguq123, jhko, charmingwc, hpark}@sogang.ac.kr

ABSTRACT

Speech restoration in real-world conditions is challenging due to compounded distortions such as clipping, band-pass filtering, digital artifacts, noise, and reverberation, and low sampling rates. Existing systems, including vocoder-based approaches, often sacrifice signal fidelity, while diffusion models remain impractical for streaming. Moreover, most assume a fixed target sampling rate, requiring external resampling that leads to redundant computations. We present TF-Restormer, an encoder-decoder architecture that concentrates analysis on input-bandwidth with a time-frequency dual-path encoder and reconstructs missing high-frequency bands through a light decoder with frequency extension queries. It enables efficient and universal restoration across arbitrary input-output rates without redundant resampling. To support adversarial training across diverse rates, we introduce a shared sampling-frequency-independent (SFI) STFT discriminator. TF-Restormer further supports streaming with a causal time module, and improves robustness under extreme degradations by injecting spectral inductive bias into the frequency module. Finally, we propose a scaled log-spectral loss that stabilizes optimization under severe conditions while emphasizing well-predicted spectral details. As a single model across sampling rates, TF-Restormer consistently outperforms prior systems, achieving balanced gains in signal fidelity and perceptual quality, while its streaming mode maintains competitive performance for real-time use. Anonymous code and demos are available at <https://tf-restormer.github.io/demo>.

1 INTRODUCTION

Speech enhancement (Ephraim & Malah, 1984; Pascual et al., 2017) has historically progressed through isolated sub-tasks with dedicated models such as denoising (Hu et al., 2020; Ho et al., 2020), dereverberation (Han et al., 2015; Wang & Wang, 2020), declipping (Mack & Habets, 2019), and bandwidth extension or super-resolution (Liu et al., 2022a; Lee & Han, 2021). In real-world settings, however, multiple distortions often coincide and are further compounded by digital distortions including lossy codecs (e.g., MP3, Ogg). These factors obscure magnitude and phase in the signal, making coherent, faithful speech restoration substantially more difficult.

This growing complexity has prompted a shift towards *general speech restoration* using generative models to handle diverse distortions (Liu et al., 2022b; Serrà et al., 2022). Vocoder (Kumar et al., 2019; Kong et al., 2020a)-based approaches reconstruct waveforms from compressed representations (Liu et al., 2022b; Andreev et al., 2022; Babaev et al., 2024). While such approaches improve perceptual quality, they discard phase information and treat speech as a semantic abstraction rather than a physical signal, producing output signals that deviate significantly from the input. In contrast, waveform-based generative models (Oord et al., 2016; Serrà et al., 2022) including GAN- and diffusion-based methods operate directly on the waveform, avoiding the abstraction bottleneck. Diffusion models (Welker et al., 2022; Richter et al., 2023) directly generate waveforms or spectra with improved fidelity, but their temporal compression or iterative sampling precludes streaming.

A further limitation of existing approaches lies in their assumption of a fixed target sampling rate. Restoration models, as well as dedicated super-resolution methods (Kim et al., 2024; Lu et al.,

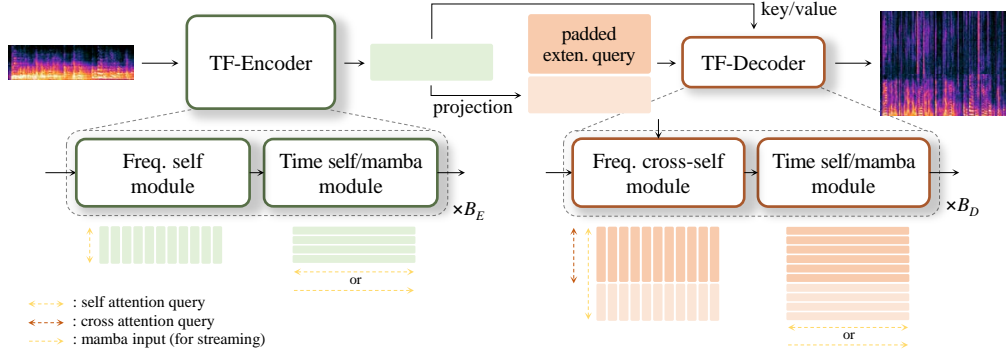


Figure 1: **Overview of TF-Restormer.** The model adopts an encoder-decoder design: TF-Encoder performs input-bandwidth analysis through stacked time and frequency modules, while the TF-Decoder reconstructs missing high-frequency bands with lightweight processing and learnable extension queries.

2025), invariably begin by resampling the input to the target rate before processing. This design choice simplifies model training but introduces critical drawbacks: every input must be converted to the highest rate regardless of its native bandwidth, leading to redundant computation from resampling. Moreover, supporting multiple output rates requires either training separate models or repeatedly upsampling and downsampling, both of which are inefficient and impractical in real-world applications. These limitations call for a universal framework that analyzes input bandwidth directly and flexibly synthesizes arbitrary output rates without external resampling.

On the other hand, for denoising and separation tasks, models have been developed primarily in the complex STFT domain (Choi et al., 2018; Hu et al., 2020). In particular, recent works introduced time-frequency (TF) dual-path models (Dang et al., 2022; Wang et al., 2023), alternating sequence modeling along time and frequency axes. This design has proved effective for enhancement and separation tasks by preserving the frequency structure, and it naturally supports sampling-frequency-independent (SFI) formulations (Paulus & Torcolli, 2022; Zhang et al., 2023), since frequency bins can be treated as sequences whose length scales with the input rate while maintaining a consistent STFT frame duration. However, despite this flexibility, existing models still assume matched input-output rates. Moreover, because TF dual-path models explicitly preserve fine spectral structure, their computational cost grows substantially with higher sampling rates, making it difficult to apply to super-resolution tasks directly.

These limitations suggest the need for a new design that retains the strengths of TF dual-path processing while overcoming the inefficiency of fixed input-output rates. To this end, we present TF-Restormer, an encoder-decoder architecture for robust speech restoration under diverse degradations. Inspired by masked autoencoders (MAE) (He et al., 2022), TF-Restormer concentrates heavy processing in a TF dual-path encoder that analyzes the input bandwidth, while a lightweight decoder reconstructs the missing high-frequency components through learnable *extension queries* (Figure 1) with *cross-self* attention mechanism (Gupta et al., 2023). This *asymmetric* design enables arbitrary input-output sampling rates without external resampling, which minimizes redundant computation.

In summary, our contributions are as follows:

- We design an *asymmetric encoder-decoder* framework based on a TF dual-path Transformer with SFI-STFT: the encoder focuses on the input bandwidth, while the lightweight decoder extends high frequencies via learnable queries with a cross-self mechanism. This design enables general speech restoration, including super-resolution across arbitrary input-output rates without external resampling, with a *shared SFI-STFT discriminator* that supports unified adversarial training across diverse rates.
- We improve robustness and practicality of TF dual-path processing by enhancing the frequency module with a projection-based *spectral inductive bias* and extending the time module to a causal variant for *streaming*, ensuring stable operation under extreme degradations as well as real-time applicability.
- We propose the *scaled log-spectral loss* as an auxiliary spectral objective that replaces conventional ℓ_1/ℓ_2 spectral objectives and complements perceptual (Babaei et al., 2024) and adversarial training (Mao et al., 2017). By selectively emphasizing reliably predictable regions, this loss stabilizes optimization under severe distortions while mitigating oversmoothing.

2 RELATED WORK

Vocoder-based restoration Vocoder systems typically project speech into Mel features (Liu et al., 2022b; Babaev et al., 2024) or learned representations (Koizumi et al., 2023; Li et al., 2024) and synthesize waveforms with neural vocoders (Oord et al., 2016; Kumar et al., 2019; Kong et al., 2020a). They often achieve “studio-like” perceptual quality but reduce fidelity, since intermediate features serve as perceptual cues rather than physical signals. Most also rely on temporally compressed U-Net structures (Pascual et al., 2017; Stoller et al., 2018), limiting real-time use. In contrast, we directly predict complex STFTs within a TF dual-path structure, retaining both magnitude and phase while enabling a streaming variant with minimal changes. Recent studies (Kaneko et al., 2022; Lu et al., 2025) further show that direct spectral prediction with adversarial training can rival vocoder-based generation.

Diffusion-based restoration Another approach is diffusion-based generation from waveform (Kong et al., 2020b; Serrà et al., 2022; Welker et al., 2022; Scheibler et al., 2024) or STFT inputs (Lemercier et al., 2023; Richter et al., 2023). While effective in perceptual quality, inference remains costly: even fast samplers require multiple denoising steps, hindering real-time use. Moreover, while diffusion excels at sampling diverse modes of a distribution, according to Babaev et al. (2024), speech enhancement typically seeks the most likely clean realization consistent with the observation, not a diverse set of alternatives. As a result, diffusion introduces unnecessary complexity for restoration or enhancement task. Therefore, we target a main-mode estimate via single-pass complex spectral prediction augmented with an adversarial loss for perceptual sharpness.

TF dual-path models For denoising, dereverberation, and separation, TF dual-path models (Dang et al., 2022; Cao et al., 2022) alternate sequence modeling along time and frequency, preserving spectral structure and supporting SFI designs (Zhang et al., 2023). They show strong performance in enhancement (Cao et al., 2022; Lu et al., 2023; Chao et al., 2024) and separation (Wang et al., 2023; Saijo et al., 2024; Shin et al., 2025), where the speech signal remains largely preserved, so prior models used identical block designs for time and frequency without considering domain-specific differences. Under challenging degradations, we address this with a projection-based frequency module that injects spectral inductive bias for more robust high-frequency recovery. In addition, while prior dual-path models assumed matched input-output rates, we extend them with an encoder-decoder structure that supports super-resolution beyond fixed-rate restoration.

Audio super-resolution Conventional bandwidth extension and super-resolution models (Liu et al., 2022a; Han & Lee, 2022; Kim et al., 2024; Lu et al., 2025) typically assume a fixed target rate, upsampling all inputs before processing to fill missing bands. While effective, this introduces redundant computation and ties each model to a single output rate, requiring repeated downsampling of outputs for different targets. In contrast, our encoder-decoder framework confines heavy processing to the input bandwidth and restores missing high-frequency bands through lightweight extension queries, improving efficiency. Unlike prior work restricted to predetermined rates, our design naturally supports user-specified outputs through the TF dual-path backbone, offering flexibility and enabling training with data from diverse native sampling rates.

3 TF-RESTORMER

3.1 SFI INPUT-OUTPUT FORMULATION

As an SFI model (Paulus & Torcoli, 2022), TF-Restormer addresses arbitrary input sampling rates f_E by constructing the STFT with a constant frame duration (SFI-STFT). Unlike conventional SFI that assumes matched input-output rates, we introduce the first decoupled formulation, enabling inference at user-specified output rates f_D . Concretely, given an input $x \in \mathbb{R}^{1 \times N_E}$ with sampling rate f_E , its STFT is $\mathbf{X} \in \mathbb{R}^{F_E \times T \times 2}$, where F_E and T are the number of frequency bins and frames. TF-Restormer then predicts $\mathbf{Y} \in \mathbb{R}^{F_D \times T \times 2}$ corresponding to an output $y \in \mathbb{R}^{1 \times N_D}$ at sampling rate f_D , satisfying $f_E : f_D = (F_E - 1) : (F_D - 1)$ under the assumption of consistent frame duration.

To ensure universal applicability across sampling rates, we adopt a 40 ms analysis window with a 20 ms hop. This choice is a common unit in speech analysis and, being integer multiples across typical rates, guarantees consistent STFT construction at $\{8, 16, 22.05, 24, 32, 44.1, 48\}$ kHz without requiring resampling. The maximum number of frequency bins F_{\max} is 961 for $f_E = 48$ kHz.

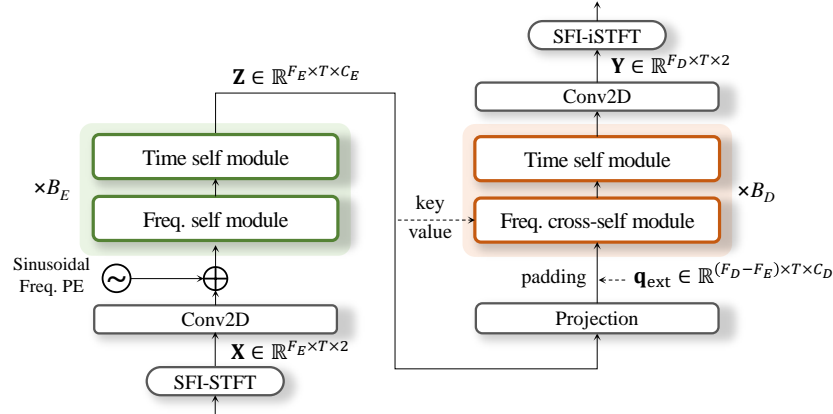


Figure 2: **Overall architecture of TF-Restormer.** With SFI-STFT and iSTFT, arbitrary input-output sample rates can be addressed in a single model. The encoder feature serves as both the input and the fixed key/value for the Freq. cross-self module in the TF-Decoder.

3.2 ANALYSIS ENCODER AND EXTENSION DECODER

TF-encoder for input analysis As illustrated in Figure 1 and 2, the TF-Restormer is constructed with TF-encoder and TF-decoder. The TF-encoder is responsible for analyzing the speech component from the input signals $\mathbf{X} \in \mathbb{R}^{F_E \times T \times 2}$. Before the TF-encoder, the input complex representation $\mathbf{X} \in \mathbb{R}^{F_E \times T \times 2}$ is first projected to C_E dimension by 2d convolution (Conv2D) layer with kernel size of (3,3), followed by layer normalization (LN) (Ba et al., 2016). Then, sinusoidal positional embeddings are added along the frequency axis (Freq. PE). In the encoder, the projected feature is alternately processed by freq and time modules B_E times to capture speech component.

TF-decoder with extension query Then, the encoder features $\mathbf{Z} \in \mathbb{R}^{F_E \times T \times C_E}$ are embedded to both the input of decoder by projection layer and key/value for cross-attention in the frequency cross-self module as shown in Figure 2. Then, the projected encoder features are padded with learnable extension query $\mathbf{q}_{\text{ext}} \in \mathbb{R}^{(F_D - F_E) \times T \times C_D}$ whose values are shared across all the frames and processed by frequency and time module by B_D times. In particular, the frequency module performs cross-attention based on encoder feature as key/value. Then, the complex STFT values $\mathbf{Y} \in \mathbb{R}^{F_D \times T \times 2}$ are estimated from decoder features by Conv2D layer.

3.3 ASYMMETRIC TF DUAL-PATH MODULE

In TF dual-path modules, given the feature with shape of $\mathbb{R}^{T \times F \times C}$ where $F \in \{F_E, F_D\}$, time modules process F independent sequences with lengths of T while frequency modules consider the feature as T sequences with lengths of F as illustrated in Figure 1. However, frequency bins are usually more static and structured sequence with a fixed length compared to time frames, exhibiting a relatively consistent structural roles. Therefore, we introduce a frequency module with projection-based inductive bias, explicitly encoding structural regularities across frequency bins for stable restoration.

We adopt common structure for both time and frequency modules borrowing from TF-Locoformer (Saijo et al., 2024). As shown in Figure 3, it consists of two macaron-style (Lu* et al., 2019) convolution feed-forward network (ConvFFN) with Conv1D with kernel size of K for capturing local contexts. In ConvFFN, the expansion factor is 3 with SwiGLU as hidden activation. Between ConvFFN modules, multi-head self-attention (MHSA) is used for global contexts with H heads. The time module performs MHSA on temporal frames with rotary positional encoding (RoPE) (Su et al., 2024) to offer the relative positions while the frequency module applies MHSA on frequency bins with the frequency projection layer to induce the structural bias.

Frequency cross-self module For frequency cross-self module, we replace the first F-ConvFFN in the frequency self module with multi-head cross-attention (MHCA) based on key-value from the encoder feature \mathbf{Z}_{enc} while query is high-frequency padded region by \mathbf{q}_{ext} , inspired by cross-self attention (Gupta et al., 2023). Therefore, MHCA conditionally operates when $f_E < f_D$ and extension query is padded, otherwise, bypassed.

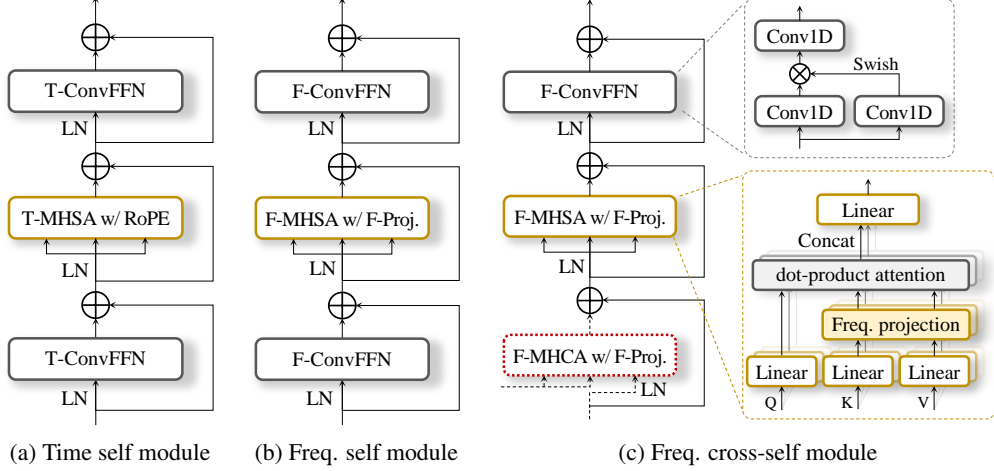


Figure 3: **Unit modules in TF-Encoder and TF-Decoder.** The (a) time module is based on MHSA with RoPE while (b) the frequency encoder module is based on MHSA with frequency projection layer. (c) The frequency decoder module employs MHCA based on key/value from the encoder features

Attention with structural bias Linformer (Wang et al., 2020) introduced linear projections of key-value to reduce the computations of attention, while MLP-Mixer (Tolstikhin et al., 2021) went further by replacing MHSA with static linear operations. Motivated by these insights, we incorporate a frequency linear projection (Fig. 3(c)) to impose an inductive bias for the structural consistency of frequency bins on top of the benefits of dynamic attention. Since frequency bins exhibit consistent characteristics, we share the same projection layer across all modules and key-value mappings. Formally, for each head $h = 1, \dots, H$, given key-value $\mathbf{K}_{h,c}, \mathbf{V}_{h,c} \in \mathbb{R}^{T \times F}$ at channel c , a learnable projection matrix $\mathbf{A}_h \in \mathbb{R}^{F_{\max} \times F_{\text{proj}}}$ with dimension F_{proj} and maximum bins F_{\max} is applied as

$$\tilde{\mathbf{K}}_{h,c} = [\mathbf{K}_{h,c}, \mathbf{O}] \mathbf{A}_h \in \mathbb{R}^{T \times F_{\text{proj}}}, \quad 1 \leq c \leq C_h, \quad (1)$$

$$\tilde{\mathbf{V}}_{h,c} = [\mathbf{V}_{h,c}, \mathbf{O}] \mathbf{A}_h \in \mathbb{R}^{T \times F_{\text{proj}}}, \quad 1 \leq c \leq C_h, \quad (2)$$

where $\mathbf{O} \in \mathbb{R}^{T \times (F_{\max} - F)}$ is a zero-padding matrix.

Streaming mode with mamba The modular design of TF dual-path model further enables a seamless extension to streaming mode by replacing the time module with Mamba (Gu & Dao, 2024) blocks. Refer to Appendix C for detailed model configurations.

4 TRAINING

The model is trained by two phases of pretraining and adversarial training. The model is trained with f_D randomly selected from $\{16, 24, 44.1, 48\}$ kHz at each step by downsampling target speech signals from VCTK dataset (Yamagishi et al., 2019). Based on speech sources, we simulated noisy reverberant signals by convolving the room impulse response (RIR) and noise samples from the DNS dataset (Reddy et al., 2020). We then applied various digital distortions including codecs and downsampled the signal to the sampling rates f_E of 8k or 16kHz, which are common in practical restoration condition (see Appendix B.1 for details).

4.1 PRETRAINING

Perceptual loss Following Babaev et al. (2024), we incorporate a self-supervised learning (SSL)-based perceptual loss to stabilize adversarial training and encourage human-aligned quality. Specifically, extracting features from a pretrained SSL model for both the enhanced and clean waveforms, we minimize the mean-squared-error between these representations:

$$\mathcal{L}_p(\theta) = \mathbb{E}_{m,n} [|\phi(g_\theta(x))_{m,n} - \phi(s)_{m,n}|^2], \quad (3)$$

given that $y = g_\theta(x)$ is output of restoration model $g_\theta(\cdot)$ with parameters of θ . $\phi(\cdot)_{m,n}$ denotes the m -th element of n -th frame from its feature map. We utilize WavLM-conv (Chen et al., 2022) as in the previous study (Babaev et al., 2024).

Proposed scaled log-spectral loss Because the perceptual loss is restricted to 16 kHz and it is beneficial to guide spectral details to complement the looseness of perceptual loss, a previous work adopted an ℓ_1 distance on the magnitude spectrum (Babaev et al., 2024). However, because TF-Restormer operates directly on the complex spectrum, the model can be explicitly supervised on both real and imaginary components in addition to the magnitude. Therefore, when denoting the STFT of target signal s by $S_{m,tf} = |S_{r,tf} + jS_{i,tf}|$ and that of model’s predicted signal $g_\theta(x)$ by $Y_{m,tf} = |Y_{r,tf} + jY_{i,tf}|$, we can extend to the complex domain as $\mathcal{L}_{\ell_1}(\theta) = \sum_{c \in \mathcal{C}} \alpha_c \cdot \mathbb{E}_{t,f} [|Y_{c,tf} - S_{c,tf}|]$, where $\mathcal{C} = \{r, i, m\}$ denotes the component index set and α_c are component weights.

However, even with complex supervision, while some regions are relatively easy to predict and receive consistent gradients, severely degraded or missing high-frequency regions yield unstable gradients and drive the model toward oversmoothing, or averaging, effects (Babaev et al., 2024). To address this, we propose a *scaled log-spectral loss* selectively emphasizing well-predicted regions while preventing poorly predicted regions from dominating:

$$\mathcal{L}_s(\theta) = \sum_{c \in \mathcal{C}} \alpha_c \cdot \mathbb{E}_{t,f} \left[w_{tf} \log \left(1 + \frac{|Y_{c,tf} - S_{c,tf}|}{w_{tf}} \right) \right], \quad (4)$$

where w_{tf} is scale factor that controls the relative scaling of gradient. The formulation $w \log(1 + d/w)$ formulation ensures large gradients on smaller distance d than w , preserving regions where phase and magnitude are already reconstructed well, while suppressing the influence of large deviations, avoiding the averaging common in ℓ_1 or ℓ_2 losses. For choosing the weight value w_{tf} , we observed that a distance $|Y_{c,tf} - S_{c,tf}|$ tends to be proportional to the scale of the corresponding source component $S_{m,tf}$. Therefore, w_{tf} is empirically set to $E[S_{m,tf}]$ by averaging over the frames. We use $\alpha_m = 0.6$, $\alpha_r = 0.2$, and $\alpha_i = 0.2$. Finally, when combined with the perceptual loss, our proposed objective becomes

$$\mathcal{L}_{\text{pre}}(\theta) = \lambda_p \mathcal{L}_p(\theta) + \lambda_s \mathcal{L}_s(\theta). \quad (5)$$

where λ_* denote loss weighting factors. Therefore, perceptual loss mainly focuses on largely deviated component while the scaled log-spectral more on well-predicted component, making them complementary to each other. For pretraining, we train the TF-Restormer with $\lambda_p = 100$ and $\lambda_s = 1$.

4.2 ADVERSARIAL TRAINING

After pretraining the generator with \mathcal{L}_{pre} , we introduce an adversarial loss component to reduce the artifacts and predict severely distorted or missing components. For adversarial training, we attach multi-scale STFT discriminators (Défossez et al., 2023) as i -th discriminator of φ_i and apply least square GAN (LS-GAN) loss (Mao et al., 2017). For generator, generator LS-GAN and feature-matching loss (Kumar et al., 2019) terms are added, respectively:

$$\mathcal{L}_{\text{gen}}(\theta) = \lambda_g \mathcal{L}_g(\theta) + \lambda_{\text{fm}} \mathcal{L}_{\text{fm}}(\theta) + \lambda_p \mathcal{L}_p(\theta) + \lambda_s \mathcal{L}_s(\theta) + \lambda_{\text{hf}} \mathcal{L}_{\text{hf}}(\theta), \quad (6)$$

$$\mathcal{L}_{\text{disc}}(\varphi_i) = \mathcal{L}_d(\varphi_i), \quad i = 1, \dots, I. \quad (7)$$

where $\mathcal{L}_{\text{hf}} = \mathcal{L}_{\text{pesq}} + 10 \cdot \mathcal{L}_{\text{utmos}}$ is additional human-feedback loss (Babaev et al., 2024) for aesthetic quality with differentiable PESQ loss¹ and UTMOS loss (Saeki et al., 2022). We performed adversarial training using $\mathcal{L}_{\text{gen}}(\theta)$ with $\lambda_g = 0.005$, $\lambda_{\text{fm}} = 0.1$, $\lambda_p = 100$, $\lambda_s = 1$, and $\lambda_{\text{hf}} = 0.0001$. Notably, we assign small weights to \mathcal{L}_g and \mathcal{L}_{hf} to avoid excessive generation artifacts. (See Appendix B.2 for details of training configuration.)

Proposed multi-scale SFI-STFT discriminators In conventional adversarial training, a dedicated generator for each target sampling rate is trained with a corresponding discriminator as well (Défossez et al., 2023; Babaev et al., 2024; Ju et al., 2024). For stable training of a single generator across diverse rates, we propose a discriminator based on SFI-STFT, which preserves a consistent physical frame duration across sampling rates. Implemented with strided Conv2D layers, STFT discriminator (Défossez et al., 2023) produces two-dimensional maps that provide local real/fake supervision in the time-frequency plane. This design maintains sensitivity to spectral structure while remaining agnostic to absolute frequency resolution, thereby supporting adversarial training across different rates without redundant resampling or multiple discriminators. We employ 5 SFI discriminators with STFT window durations of $\{20, 40, 60, 80, 100\}$ ms.

¹<https://github.com/audiolabs/torch-pesq>

5 EVALUATION

5.1 DATASET AND METRICS

UNIVERSE data for speech restoration As speech restoration model, we evaluate on 100 synthetic samples generated by UNIVERSE authors (Serrà et al., 2022) to ensure comparability to prior works in $f_E = f_D = 16\text{kHz}$ setting. The dataset introduces diverse simulated degradations such as bandpass filtering, reverberation, codec compression, and transmission artifacts.

VCTK-DEMAND for denoising We additionally evaluated the well-known Valentini denoising dataset (Valentini-Botinhao et al., 2017) for direct comparison with conventional enhancement models as speech enhancement benchmarking. The evaluation set (824 utterances) consists of noisy mixtures from two speakers under four SNR conditions (17.5, 12.5, 7.5, and 2.5 dB).

VCTK for super-resolution For super-resolution evaluation, we construct paired data by down-sampling 48 kHz clean utterances from the VCTK-0.92 dataset (Yamagishi et al., 2019). Beyond the clean case, we also create noisy-distorted conditions by adding degradations such as noise, reverberation, band-pass filtering, and codec effects, enabling a comprehensive evaluation of speech restoration with super-resolution. Note that the training simulation follows a similar procedure, which may provide a slight advantage to our model. (See Appendix D for details of the simulation.)

For the evaluation, we adopt non-intrusive perceptual estimators for mean opinion score (MOS): DNSMOS (Reddy et al., 2022), UTMOS (Saeki et al., 2022), and WVMOS (Andreev et al., 2022) to assess the perceptual quality regardless of reference signals. We also employ perceptual evaluation of speech quality (PESQ) (Rix et al., 2001) to assess the perceptual signal fidelity of restored signal compared to the reference. As a complement of PESQ based on lower band, we consider signal-to-distortion ratio (SDR) (Roux et al., 2018), log-spectral distance (LSD), and mel-cepstral distortion (MCD) (Fukada et al., 1992) to assess the full-band signal (44.1/48kHz). In addition, to evaluate the reference-aware speech generation quality by capturing semantic congruence, we report SpeechBERTScore(sBERT) and SpeechTokenDistance(sTokDis) (Saeki et al., 2024). We also confirm effectiveness on real recordings based on DNSMOS, UTMOS, and WVMOS (Appendix F).

5.2 COMPARISON WITH EXISTING MODELS

For the UNIVERSE dataset, we consider VoiceFixer (Liu et al., 2022b) as a Mel vocoder-based baseline, StoRM (Lemercier et al., 2023), UNIVERSE (Serrà et al., 2022), and UNIVERSE++ (Scheibler et al., 2024) as diffusion-based baselines, TF-Locoformer as a recent TF dual-path Transformer model, and FINALLY (Babaev et al., 2024) as a latest strong Mel-vocoder method. As shown in Table 1, VoiceFixer improves MOS but sacrifices fidelity due to its Mel representation, while FINALLY achieves the highest perceptual quality yet lacks signal fidelity, a trend confirmed in Table 2. Diffusion-based methods yield more balanced results by directly operating in the waveform or complex STFT. TF-Locoformer preserves signal-level fidelity but suffers from residual perceptual artifacts and failure to recover lost details and naturalness (MOS, LSD). In contrast, TF-Restormer provides consistent improvements under fidelity, semantics, and perceptual quality, with its streaming variant maintaining competitive effectiveness under causal constraints. This indicates its robustness across diverse degradations in a universal restoration setting. Note that all the compared models are offline methods.

Table 1: Results on UNIVERSE data for general speech restoration. [†]We utilized pretrained models from implementation code from UNIVERSE++ (Scheibler et al., 2024). [‡]The results are reported in the original paper (Babaev et al., 2024)

Model	Signal fidelity				Semantic fidelity		Non-intrusive quality		
	PESQ↑	SDR↑	LSD↓	MCD↓	sBERT↑	sTokDis↑	WVMOS↑	UTMOS↑	DNSMOS↑
Input Ground Truth	1.55 4.50	5.58 ∞	1.89 0.00	10.21 0.00	0.84 1.00	0.69 1.00	1.76 4.28	2.19 4.26	2.23 3.33
VoiceFixer	1.77	-5.68	1.49	10.50	0.84	0.71	3.28	2.83	2.99
StoRM	1.76	9.01	1.67	6.87	0.84	0.70	3.14	2.70	2.94
UNIVERSE [†]	1.74	7.73	1.92	6.25	0.79	0.67	2.95	2.64	2.73
UNIVERSE++ [†]	1.80	8.42	1.76	5.96	0.81	0.69	3.19	2.71	2.82
TF-Locoformer	2.13	11.61	2.00	6.26	0.89	0.76	3.20	2.95	2.86
FINALLY	-	-	-	-	-	-	4.43[‡]	4.21[‡]	3.25 [‡]
TF-Restormer	2.30	11.12	1.45	5.08	0.91	0.80	4.34	4.08	3.25
TF-Restormer- <i>streaming</i>	2.00	8.89	1.47	6.01	0.87	0.74	3.93	3.77	3.14

Next, we evaluate TF-Restormer on the VCTK+DEMAND focusing on denoising. In Table 2, we compare against DB-AIAT (Yu et al., 2021), MP-SENet (Lu et al., 2023), and TF-Locoformer as dedicated denoising models, and VoiceFixer, UNIVERSE, and FINALLY as universal restoration baselines. Since the input speech is already well preserved and only corrupted by additive noise, it favors models that minimize unnecessary generation and faithfully retain the input signal. Accordingly, dedicated denoising models outperform universal restoration models in terms of signal fidelity, as they are optimized to suppress noise without altering intact regions. In contrast, restoration models risk degrading reliability by over-modifying clean inputs, making them less trustworthy for such simple cases. While not surpassing dedicated denoising models in raw signal metrics, TF-Restormer achieves more consistent semantic and perceptual gains, showing strong generalization despite being designed for universal restoration.

Table 2: Results on VCTK-DEMAND for denoising task.

Model	Signal fidelity				Semantic fidelity		Non-intrusive quality		
	PESQ↑	SDR↑	LSD↓	MCD↓	sBERT↑	sTokDis↑	WVMOS↑	UTMOS↑	DNMSMOS↑
Input	1.98	8.56	1.27	5.40	0.91	0.82	3.01	2.90	2.45
Ground Truth	4.50	∞	0.00	0.00	1.00	1.00	4.52	4.07	3.16
DB-AIAT	3.27	21.30	0.90	1.77	0.95	0.87	4.39	3.83	3.13
MP-SENet	3.61	21.03	0.85	1.58	0.95	0.88	4.35	3.86	3.12
TF-Locoformer	3.30	23.82	0.92	3.58	0.95	0.87	4.66	3.93	3.20
VoiceFixer	2.40	-1.12	0.97	7.40	0.90	0.81	4.15	3.50	3.08
UNIVERSE	2.84	18.77	1.17	2.20	0.92	0.83	4.32	3.75	3.03
FINALLY	2.94	4.60	-	-	-	4.87	4.32	3.22	
TF-Restormer	3.41	19.45	0.75	1.54	0.95	0.88	4.75	4.14	3.14
TF-Restormer- <i>streaming</i>	2.89	16.43	0.85	2.16	0.93	0.84	4.56	4.05	3.09

Finally, we experiment on the super-resolution task in Table 3, using a single model that directly supports arbitrary output sampling rates. For clean cases, we compare against dedicated super-resolution models: NVSR (Liu et al., 2022a), Frepainter (Kim et al., 2024), and AP-BWE (Lu et al., 2025), as well as VoiceFixer as a universal restoration baseline. As in Table 2, since the low-band of the input speech remains intact, dedicated models that concentrate on reconstructing the upper bands are favored. Unlike conventional approaches that rely on fixed input-output rates and often require zero-padding or redundant resampling, TF-Restormer leverages extension queries to dynamically expand the spectrum. With this versatility, TF-Restormer shows stable performance comparable to the dedicated models, faithfully retaining clean low-frequency regions while effectively generating high-frequency components. In addition, under noisy-distorted conditions, TF-Restormer simultaneously restores corrupted regions and reconstructs missing high bands, demonstrating robust generalization beyond pure super-resolution. Overall, these results suggest the advantage of our model as a universal restoration framework that achieves bandwidth extension without sacrificing signal fidelity or requiring explicit resampling.

Table 3: Results on VCTK for super-resolution under clean and noisy-distorted conditions. [†]The models require fixed output sampling rates f' , thus evaluated by upsampling the input of f_E to $f' \geq f_D$ and downsampling the output back to the target rate f_D . [‡]Dedicated models trained specifically for $f_D = 16\text{kHz}$.

Method	8kHz → 16kHz			8kHz → 24kHz			8kHz → 44.1kHz			16kHz → 48kHz		
	LSD↓	MCD↓	UTMOS↑	LSD↓	MCD↓	UTMOS↑	LSD↓	MCD↓	UTMOS↑	LSD↓	MCD↓	UTMOS↑
<i>clean (super-resolution only)</i>												
Input	2.53	1.84	3.33	2.91	2.03	3.33	3.44	2.44	3.33	3.17	1.31	3.83
NVSR [†]	0.83	1.62	3.64	0.89	1.82	3.64	0.94	2.06	3.64	-	-	-
Frepainter [†]	1.33	1.63	3.64	1.40	1.97	3.64	1.37	2.37	3.64	1.31	1.43	3.80
AP-BWE [†]	0.90 [‡]	1.33 [‡]	3.56 [‡]	0.86	1.36	3.67	0.88	1.58	3.67	0.85	1.38	3.75
VoiceFixer [†]	1.05	6.78	3.49	1.05	6.49	3.49	1.06	6.11	3.49	-	-	-
TF-Restormer	0.89	1.29	4.10	0.95	1.48	4.09	1.01	1.74	4.10	0.97	1.28	4.11
<i>Noisy-distorted (general speech restoration + super-resolution)</i>												
Input	3.36	11.38	1.73	3.49	11.60	1.73	3.64	11.47	1.73	3.48	11.37	1.73
VoiceFixer [†]	1.36	7.62	2.97	1.35	7.32	2.97	1.40	6.96	2.97	-	-	-
StoRM	1.76	4.57	2.57	-	-	-	-	-	-	-	-	-
UNIVERSE++	1.79	5.28	2.49	-	-	-	-	-	-	-	-	-
TF-Restormer	1.16	2.78	4.22	1.21	2.97	4.22	1.18	3.08	4.21	1.18	2.86	4.22
TF-Restormer- <i>streaming</i>	1.30	3.93	3.96	1.31	4.01	3.99	1.30	4.05	4.02	1.26	3.86	4.05

Table 4: Ablation Study. VCTK-C and -ND denote clean and noisy-distorted input from VCTK data in Table 3.

Loss	PESQ↑	MCD↓	UTMOS↑	Case	LSD↓	MCD↓	UTMOS↑	Case	PESQ↑	MCD↓	UTMOS↑
UNIVERSE (general restoration)											
Mag.-only	2.07	6.03	3.82	VCTK-C (super-resol., 8 → 16kHz)	2.12	2.93	3.82	w/o F-proj.	2.26	5.56	3.90
Mag.+Cplx.	2.23	5.70	3.76	Dec-only.	1.04	1.81	4.07	w/ F-proj.	2.29	4.96	4.10
Scaled log	2.29	4.96	4.10	w/ MHCA	0.89	1.29	4.10	VCTK+DEMAND (denoising)			
VCTK+DEMAND (denoising)											
Mag.-only	2.93	3.13	3.95	VCTK-C (super-resol., 8 → 44.1kHz)	3.25	10.48	3.36	w/o F-proj.	3.21	0.85	4.03
Mag.+Cplx.	2.97	2.98	3.87	Dec-only.	1.35	1.70	4.07	w/ F-proj.	3.41	0.75	4.14
Scaled log	3.41	1.54	4.14	w/ MHCA	1.01	1.74	4.10	VCTK-C (super-resol., 8 → 16kHz)			
VCTK-C (super-resol., 8 → 16kHz)											
Mag.-only	3.42	2.10	4.10	VCTK-ND (super-resol., 8 → 16kHz)	2.23	4.39	3.77	w/o F-proj.	3.54	1.68	3.97
Mag.+Cplx.	3.48	1.86	4.07	Dec-only.	1.20	3.30	4.11	w/ F-proj.	3.70	1.29	4.11
Scaled log	3.70	1.29	4.10	w/ MHCA	1.16	2.78	4.22	(c) Effects of frequency projection			

(a) Effect of scaled log-spectral loss

(b) Decoder design

5.3 ABLATION STUDY

To validate the effects of the proposed methods, we conduct an ablation study on scaled log-spectral loss, decoder design, and frequency projection module.

Effects of scaled log-spectral loss. First, we compare the scaled log-spectral (S-log) loss against two other regression losses as a auxiliary objective to the perceptual loss: ℓ_1 loss on magnitude of STFT (Mag.-only) as in (Babaev et al., 2024) and ℓ_1 loss on real, imaginary, and magnitude (Cplx.) for STFT. In Table 4a, using a complex loss shows the better results than only guiding magnitude component for all the cases. Also, using the proposed scaled log-spectral loss further improved the performance by stabilizing the gradients, confirming that finer spectral detail can be preserved without sacrificing global fidelity.

Decoder design. Next, we validate our encoder-decoder design when $f_E \neq f_D$. Compared to the proposed method with MHCA, we test two variants: (i) a large decoder without an encoder, where extension queries are padded at the input, and (ii) an encoder-decoder without MHCA, where the decoder shares the same block design as the encoder. All three cases converge to similar behavior when $f_E = f_D$. For fairness, we rescaled the decoder-only case to match computation and memory. Illustrations are provided in Appendix E. As shown in Table 4b, the encoder-decoder design yields more stable improvements by focusing computation on the input bandwidth. The decoder-only case produces unstable results in full-band reconstruction (8 → 44.1kHz). Adding the cross-self frequency module further improves performance: high-frequency bands are reconstructed more reliably via cross-attention using encoder features, whereas the isotropic encoder-decoder relies only on self-attention and thus performs worse.

Effects of frequency projection. Finally, we examine the effect of the frequency projection module on robustness. Without projection, RoPE provides only positional context, resulting in the conventional symmetric TF dual-path structure. In contrast, adding projection to F-MHSA imposes structural bias along the frequency axis, yielding more stable training and consistent improvements across tasks, particularly under severe distortions and during high-frequency extension. These results demonstrate that structural bias is valuable for robust restoration under extreme conditions.

6 CONCLUSION

We presented TF-Restormer, a speech restoration model with an encoder-decoder design that enables efficient operation across arbitrary input and output sampling rates. By concentrating on the input bandwidth with a strong TF dual-path encoder and extending high frequencies through lightweight decoder queries with a cross-self mechanism, TF-Restormer achieves balanced improvements in both signal- and semantic-level fidelity while also showing robust performance on single-task benchmarks such as denoising and bandwidth extension. We also proposed a shared SFI-STFT discriminator for unified adversarial training across diverse sampling rates. Together, these results establish TF-Restormer as a universal and practical framework for robust speech restoration across diverse sampling conditions.

REPRODUCIBILITY STATEMENT

We make our implementation code and demo anonymously accessible. Our anonymous link for pre-trained TF-Restormer and inference code is also included in demo pages: <https://tf-restormer.github.io/demo>

ETHICS STATEMENT

We use only public speech corpora and collect no new personal data. We do not attempt speaker re-identification, and we do not redistribute raw audio. Aware of potential misuse (e.g., covert monitoring), we will apply access controls and intended-use restrictions and require legal compliance for any release.

REFERENCES

Pavel Andreev, Aibek Alanov, Oleg Ivanov, and Dmitry Vetrov. Hifi++: a unified framework for bandwidth extension and speech enhancement. *arXiv preprint arXiv:2203.13086*, 2022.

Jimmy Lei Ba, Jamie Ryan Kiros, and Geoffrey E. Hinton. Layer normalization, 2016.

Nicholas Babaev, Kirill Tamogashev, Azat Saginbaev, Ivan Shchekotov, Hanbin Bae, Hosang Sung, WonJun Lee, Hoon-Young Cho, and Pavel Andreev. FINALLY: fast and universal speech enhancement with studio-like quality. In *The Thirty-eighth Annual Conference on Neural Information Processing Systems*, 2024. URL <https://openreview.net/forum?id=18RdkSv9h9>.

Ruizhe Cao, Sherif Abdulatif, and Bin Yang. CMGAN: Conformer-based Metric GAN for Speech Enhancement. In *Proc. Interspeech*, pp. 936–940, 2022. doi: 10.21437/Interspeech.2022-517.

Rong Chao, Wen-Huang Cheng, Moreno La Quatra, Sabato Marco Siniscalchi, Chao-Han Huck Yang, Szu-Wei Fu, and Yu Tsao. An investigation of incorporating mamba for speech enhancement. *arXiv preprint arXiv:2405.06573*, 2024.

Sanyuan Chen, Chengyi Wang, Zhengyang Chen, Yu Wu, Shujie Liu, Zhuo Chen, Jinyu Li, Naoyuki Kanda, Takuya Yoshioka, Xiong Xiao, et al. WavLM: Large-scale self-supervised pre-training for full stack speech processing. *IEEE Journal of Selected Topics in Signal Processing*, 16(6):1505–1518, 2022.

Heeong-Seok Choi, Jang-Hyun Kim, Jaesung Huh, Adrian Kim, Jung-Woo Ha, and Kyogu Lee. Phase-aware speech enhancement with deep complex u-net. In *Proc. Int. Conf. Learn. Represent. (ICLR)*, 2018.

Feng Dang, Hangting Chen, and Pengyuan Zhang. DPT-FSNet: Dual-Path Transformer Based Full-Band and Sub-Band Fusion Network for Speech Enhancement. In *Proc. IEEE Int. Conf. Acoust., Speech Signal Process. (ICASSP)*, pp. 6857–6861, 2022. doi: 10.1109/ICASSP43922.2022.9746171.

Alexandre Défossez, Nicolas Usunier, Léon Bottou, and Francis Bach. Music source separation in the waveform domain. *arXiv preprint arXiv:1911.13254*, 2019.

Alexandre Défossez, Jade Copet, Gabriel Synnaeve, and Yossi Adi. High fidelity neural audio compression. *Transactions on Machine Learning Research*, 2023. ISSN 2835-8856. URL <https://openreview.net/forum?id=ivCd8z8zR2>. Featured Certification, Reproducibility Certification.

Yariv Ephraim and David Malah. Speech enhancement using a minimum-mean square error short-time spectral amplitude estimator. *IEEE Transactions on acoustics, speech, and signal processing*, 32(6):1109–1121, 1984.

T. Fukada, K. Tokuda, T. Kobayashi, and S. Imai. An adaptive algorithm for mel-cepstral analysis of speech. In *[Proceedings] ICASSP-92: 1992 IEEE International Conference on Acoustics, Speech, and Signal Processing*, volume 1, pp. 137–140 vol.1, 1992. doi: 10.1109/ICASSP.1992.225953.

Albert Gu and Tri Dao. Mamba: Linear-time sequence modeling with selective state spaces. In *First Conference on Language Modeling*, 2024. URL <https://openreview.net/forum?id=tEYskw1VY2>.

Agrim Gupta, Jiajun Wu, Jia Deng, and Li Fei-Fei. Siamese masked autoencoders. In *Thirty-seventh Conference on Neural Information Processing Systems*, 2023. URL <https://openreview.net/forum?id=yC3q7vInux>.

Kun Han, Yuxuan Wang, DeLiang Wang, William S. Woods, Ivo Merks, and Tao Zhang. Learning spectral mapping for speech dereverberation and denoising. *IEEE/ACM Transactions on Audio, Speech, and Language Processing*, 23(6):982–992, 2015. doi: 10.1109/TASLP.2015.2416653.

Seungu Han and Junhyeok Lee. Nu-wave 2: A general neural audio upsampling model for various sampling rates. In *INTERSPEECH*, pp. 4401–4405, 2022. URL <https://doi.org/10.21437/Interspeech.2022-45>.

Kaiming He, Xinlei Chen, Saining Xie, Yanghao Li, Piotr Dollár, and Ross Girshick. Masked autoencoders are scalable vision learners. In *Proceedings of the IEEE/CVF Conference on Computer Vision and Pattern Recognition (CVPR)*, pp. 16000–16009, June 2022.

Jonathan Ho, Ajay Jain, and Pieter Abbeel. Denoising diffusion probabilistic models. *Advances in Neural Information Processing Systems*, 33:6840–6851, 2020.

Yanxin Hu, Yun Liu, Shubo Lv, Mengtao Xing, Shimin Zhang, Yihui Fu, Jian Wu, Bihong Zhang, and Lei Xie. DCCRN: Deep Complex Convolution Recurrent Network for Phase-Aware Speech Enhancement. In *Proc. Interspeech*, pp. 2472–2476, 2020. doi: 10.21437/Interspeech.2020-2537.

Marco Jeub, Magnus Schafer, and Peter Vary. A binaural room impulse response database for the evaluation of dereverberation algorithms. In *2009 16th International Conference on Digital Signal Processing*, pp. 1–5, 2009. doi: 10.1109/ICDSP.2009.5201259.

Zeqian Ju, Yuancheng Wang, Kai Shen, Xu Tan, Detai Xin, Dongchao Yang, Eric Liu, Yichong Leng, Kaitao Song, Siliang Tang, Zhizheng Wu, Tao Qin, Xiangyang Li, Wei Ye, Shikun Zhang, Jiang Bian, Lei He, Jinyu Li, and sheng zhao. Naturalspeech 3: Zero-shot speech synthesis with factorized codec and diffusion models. In *Forty-first International Conference on Machine Learning*, 2024. URL <https://openreview.net/forum?id=dVhrnjZJad>.

Takuhiko Kaneko, Kou Tanaka, Hirokazu Kameoka, and Shogo Seki. Istdftnet: Fast and lightweight mel-spectrogram vocoder incorporating inverse short-time fourier transform. In *ICASSP 2022 - 2022 IEEE International Conference on Acoustics, Speech and Signal Processing (ICASSP)*, pp. 6207–6211, 2022. doi: 10.1109/ICASSP43922.2022.9746713.

Seung-Bin Kim, Sang-Hoon Lee, Ha-Yeong Choi, and Seong-Whan Lee. Audio super-resolution with robust speech representation learning of masked autoencoder. *IEEE/ACM Transactions on Audio, Speech, and Language Processing*, 32:1012–1022, 2024. doi: 10.1109/TASLP.2023.3349053.

Yuma Koizumi, Heiga Zen, Shigeki Karita, Yifan Ding, Kohei Yatabe, Nobuyuki Morioka, Yu Zhang, Wei Han, Ankur Bapna, and Michiel Bacchiani. Miipher: A robust speech restoration model integrating self-supervised speech and text representations. In *2023 IEEE Workshop on Applications of Signal Processing to Audio and Acoustics (WASPAA)*, pp. 1–5. IEEE, 2023.

Jungil Kong, Jaehyeon Kim, and Jaekyoung Bae. Hifi-GAN: Generative adversarial networks for efficient and high fidelity speech synthesis. *Advances in Neural Information Processing Systems*, 33:17022–17033, 2020a.

Zhifeng Kong, Wei Ping, Jiaji Huang, Kexin Zhao, and Bryan Catanzaro. Diffwave: A versatile diffusion model for audio synthesis. *arXiv preprint arXiv:2009.09761*, 2020b.

Kundan Kumar, Rithesh Kumar, Thibault De Boissiere, Lucas Gestin, Wei Zhen Teoh, Jose Sotelo, Alexandre De Brebisson, Yoshua Bengio, and Aaron C Courville. MelGAN: Generative adversarial networks for conditional waveform synthesis. *Advances in neural information processing systems*, 32, 2019.

Bunlong Lay, Simon Welker, Julius Richter, and Timo Gerkmann. Reducing the prior mismatch of stochastic differential equations for diffusion-based speech enhancement. *arXiv preprint arXiv:2302.14748*, 2023.

Junhyeok Lee and Seungu Han. Nu-wave: A diffusion probabilistic model for neural audio upsampling. In *Interspeech 2021*, pp. 1634–1638, 2021. doi: 10.21437/Interspeech.2021-36.

Jean-Marie Lemercier, Julius Richter, Simon Welker, and Timo Gerkmann. Storm: A diffusion-based stochastic regeneration model for speech enhancement and dereverberation. *IEEE/ACM Transactions on Audio, Speech, and Language Processing*, 2023.

Xu Li, Qirui Wang, and Xiaoyu Liu. MaskSR: Masked Language Model for Full-band Speech Restoration. In *Interspeech 2024*, pp. 2275–2279, 2024. doi: 10.21437/Interspeech.2024-1584.

Haohe Liu, Woosung Choi, Xubo Liu, Qiuqiang Kong, Qiao Tian, and DeLiang Wang. Neural vocoder is all you need for speech super-resolution. In *Interspeech 2022*, pp. 4227–4231, 2022a. doi: 10.21437/Interspeech.2022-11017.

Haohe Liu, Xubo Liu, Qiuqiang Kong, Qiao Tian, Yan Zhao, DeLiang Wang, Chuanzeng Huang, and Yuxuan Wang. Voicefixer: A unified framework for high-fidelity speech restoration. In *Interspeech 2022*, pp. 4232–4236, 2022b. doi: 10.21437/Interspeech.2022-11026.

Ilya Loshchilov and Frank Hutter. Decoupled Weight Decay Regularization. In *Proc. Int. Conf. Learn. Represent. (ICLR)*, 2019.

Ye-Xin Lu, Yang Ai, and Zhen-Hua Ling. MP-SENet: A Speech Enhancement Model with Parallel Denoising of Magnitude and Phase Spectra. In *Proc. Interspeech*, pp. 3834–3838, 2023.

Ye-Xin Lu, Yang Ai, Hui-Peng Du, and Zhen-Hua Ling. Towards high-quality and efficient speech bandwidth extension with parallel amplitude and phase prediction. *IEEE Transactions on Audio, Speech and Language Processing*, 33:236–250, 2025. doi: 10.1109/TASLP.2024.3519881.

Yiping Lu*, Zhuohan Li*, Di He, Zhiqing Sun, Bin Dong, Tao Qin, Liwei Wang, and Tie yan Liu. Understanding and improving transformer from a multi-particle dynamic system point of view. In *ICLR 2020 Workshop on Integration of Deep Neural Models and Differential Equations*, 2019. URL <https://openreview.net/forum?id=pxlqJa21C>.

Wolfgang Mack and Emanuël A. P. Habets. Declipping speech using deep filtering. In *2019 IEEE Workshop on Applications of Signal Processing to Audio and Acoustics (WASPAA)*, pp. 200–204, 2019. doi: 10.1109/WASPAA.2019.8937287.

Xudong Mao, Qing Li, Haoran Xie, Raymond YK Lau, Zhen Wang, and Stephen Paul Smolley. Least squares generative adversarial networks. In *Proceedings of the IEEE international conference on computer vision*, pp. 2794–2802, 2017.

Arsha Nagrani, Joon Son Chung, and Andrew Zisserman. VoxCeleb: a large-scale speaker identification dataset. *arXiv preprint arXiv:1706.08612*, 2017.

Satoshi Nakamura, Kazuo Hiyane, Futoshi Asano, Takanobu Nishiura, and Takeshi Yamada. Acoustical sound database in real environments for sound scene understanding and hands-free speech recognition. In M. Gavrilidou, G. Carayannis, S. Markantonatou, S. Piperidis, and G. Stainhauer (eds.), *Proceedings of the Second International Conference on Language Resources and Evaluation (LREC'00)*, Athens, Greece, May 2000. European Language Resources Association (ELRA). URL <https://aclanthology.org/L00-1264/>.

Aaron van den Oord, Sander Dieleman, Heiga Zen, Karen Simonyan, Oriol Vinyals, Alex Graves, Nal Kalchbrenner, Andrew Senior, and Koray Kavukcuoglu. WaveNet: A generative model for raw audio. *arXiv preprint arXiv:1609.03499*, 2016.

Santiago Pascual, Antonio Bonafonte, and Joan Serrà. SEGAN: Speech enhancement generative adversarial network. In *Interspeech 2017*, pp. 3642–3646, 2017. doi: 10.21437/Interspeech.2017-1428.

Jouni Paulus and Matteo Torcoli. Sampling frequency independent dialogue separation. In *2022 30th European Signal Processing Conference (EUSIPCO)*, pp. 160–164, 2022. doi: 10.23919/EUSIPCO55093.2022.9909824.

Chandan K.A. Reddy, Vishak Gopal, Ross Cutler, Ebrahim Beyrami, Roger Cheng, Harishchandra Dubey, Sergiy Matusevych, Robert Aichner, Ashkan Aazami, Sebastian Braun, Puneet Rana, Sriram Srinivasan, and Johannes Gehrke. The INTERSPEECH 2020 Deep Noise Suppression Challenge: Datasets, Subjective Testing Framework, and Challenge Results. In *Proc. Interspeech*, pp. 2492–2496, 2020. doi: 10.21437/Interspeech.2020-3038.

Chandan KA Reddy, Vishak Gopal, and Ross Cutler. Dnsmos p. 835: A non-intrusive perceptual objective speech quality metric to evaluate noise suppressors. In *ICASSP 2022-2022 IEEE International Conference on Acoustics, Speech and Signal Processing (ICASSP)*, pp. 886–890. IEEE, 2022.

Julius Richter, Simon Welker, Jean-Marie Lemercier, Bunlong Lay, and Timo Gerkmann. Speech enhancement and dereverberation with diffusion-based generative models. *IEEE/ACM Transactions on Audio, Speech, and Language Processing*, 31:2351–2364, 2023. doi: 10.1109/TASLP.2023.3285241.

A.W. Rix, J.G. Beerends, M.P. Hollier, and A.P. Hekstra. Perceptual evaluation of speech quality (PESQ)-a new method for speech quality assessment of telephone networks and codecs. In *2001 IEEE International Conference on Acoustics, Speech, and Signal Processing. Proceedings (Cat. No.01CH37221)*, volume 2, pp. 749–752 vol.2, 2001. doi: 10.1109/ICASSP.2001.941023.

Jonathan Le Roux, Scott Wisdom, Hakan Erdogan, and John R. Hershey. SDR - half-baked or well done? *CoRR*, abs/1811.02508, 2018. URL <http://arxiv.org/abs/1811.02508>.

Takaaki Saeki, Detai Xin, Wataru Nakata, Tomoki Koriyama, Shinnosuke Takamichi, and Hiroshi Saruwatari. UTMOS: Utokyo-sarulab system for voicemos challenge 2022. *arXiv preprint arXiv:2204.02152*, 2022.

Takaaki Saeki, Soumi Maiti, Shinnosuke Takamichi, Shinji Watanabe, and Hiroshi Saruwatari. SpeechBERTScore: Reference-Aware Automatic Evaluation of Speech Generation Leveraging NLP Evaluation Metrics. In *Interspeech 2024*, pp. 4943–4947, 2024. doi: 10.21437/Interspeech.2024-1508.

Kohei Saijo, Gordon Wichern, François G. Germain, Zexu Pan, and Jonathan Le Roux. Tf-locoformer: Transformer with local modeling by convolution for speech separation and enhancement. In *2024 18th International Workshop on Acoustic Signal Enhancement (IWAENC)*, pp. 205–209, 2024. doi: 10.1109/IWAENC61483.2024.10694313.

Robin Scheibler, Yusuke Fujita, Yuma Shirahata, and Tatsuya Komatsu. Universal score-based speech enhancement with high content preservation. In *Interspeech 2024*, pp. 1165–1169, 2024. doi: 10.21437/Interspeech.2024-138.

Joan Serrà, Santiago Pascual, Jordi Pons, R Oguz Araz, and Davide Scaini. Universal speech enhancement with score-based diffusion. *arXiv preprint arXiv:2206.03065*, 2022.

Ui-Hyeop Shin, Bon Hyek Ku, and Hyung-Min Park. TF-CorrNet: Leveraging spatial correlation for continuous speech separation. *IEEE Signal Processing Letters*, 32:1875–1879, 2025. doi: 10.1109/LSP.2025.3562819.

Daniel Stoller, Sebastian Ewert, and Simon Dixon. Wave-u-net: A multi-scale neural network for end-to-end audio source separation. *CoRR*, abs/1806.03185, 2018. URL <http://arxiv.org/abs/1806.03185>.

Jianlin Su, Murtadha Ahmed, Yu Lu, Shengfeng Pan, Wen Bo, and Yunfeng Liu. Roformer: Enhanced transformer with rotary position embedding. *Neurocomputing*, 568:127063, 2024. ISSN 0925-2312. doi: <https://doi.org/10.1016/j.neucom.2023.127063>. URL <https://www.sciencedirect.com/science/article/pii/S0925231223011864>.

Jiaqi Su, Zeyu Jin, and Adam Finkelstein. HiFi-GAN: High-fidelity denoising and dereverberation based on speech deep features in adversarial networks. 2020.

Jiaqi Su, Zeyu Jin, and Adam Finkelstein. HiFi-GAN-2: Studio-quality speech enhancement via generative adversarial networks conditioned on acoustic features. In *2021 IEEE Workshop on Applications of Signal Processing to Audio and Acoustics (WASPAA)*, pp. 166–170. IEEE, 2021.

Joachim Thiemann, Nobutaka Ito, and Emmanuel Vincent. The diverse environments multi-channel acoustic noise database (demand): A database of multichannel environmental noise recordings. *Proceedings of Meetings on Acoustics*, 19(1):035081, 05 2013. ISSN 1939-800X. doi: 10.1121/1.4799597. URL <https://doi.org/10.1121/1.4799597>.

Ilya Tolstikhin, Neil Houlsby, Alexander Kolesnikov, Lucas Beyer, Xiaohua Zhai, Thomas Unterthiner, Jessica Yung, Andreas Peter Steiner, Daniel Keysers, Jakob Uszkoreit, Mario Lucic, and Alexey Dosovitskiy. MLP-mixer: An all-MLP architecture for vision. In A. Beygelzimer, Y. Dauphin, P. Liang, and J. Wortman Vaughan (eds.), *Advances in Neural Information Processing Systems*, 2021. URL <https://openreview.net/forum?id=EI2KOXKdnP>.

Cassia Valentini-Botinhao et al. Noisy speech database for training speech enhancement algorithms and tts models. 2017.

Sinong Wang, Belinda Z. Li, Madien Khabsa, Han Fang, and Hao Ma. Linformer: Self-attention with linear complexity, 2020.

Zhong-Qiu Wang and DeLiang Wang. Deep learning based target cancellation for speech dereverberation. *IEEE/ACM Transactions on Audio, Speech, and Language Processing*, 28:941–950, 2020. doi: 10.1109/TASLP.2020.2975902.

Zhong-Qiu Wang, Samuele Cornell, Shukjae Choi, Younglo Lee, Byeong-Yeol Kim, and Shinji Watanabe. TF-GridNet: Integrating Full- and Sub-Band Modeling for Speech Separation. *IEEE/ACM Trans. Audio, Speech, Language Process.*, 31:3221–3236, 2023. doi: 10.1109/TASLP.2023.3304482.

Simon Welker, Julius Richter, and Timo Gerkmann. Speech enhancement with score-based generative models in the complex STFT domain. In *Proc. Interspeech 2022*, pp. 2928–2932, 2022. doi: 10.21437/Interspeech.2022-10653.

Junichi Yamagishi, Christophe Veaux, Kirsten MacDonald, et al. Cstr vctk corpus: English multi-speaker corpus for cstr voice cloning toolkit (version 0.92). 2019.

Guochen Yu, Andong Li, Yutian Wang, Yinuo Guo, Hui Wang, and Chengshi Zheng. Dual-branch attention-in-attention transformer for single-channel speech enhancement. *CoRR*, abs/2110.06467, 2021. URL <https://arxiv.org/abs/2110.06467>.

Wangyou Zhang, Kohei Saijo, Zhong-Qiu Wang, Shinji Watanabe, and Yanmin Qian. Toward Universal Speech Enhancement For Diverse Input Conditions. In *Proc. IEEE ASRU*, pp. 1–6, 2023. doi: 10.1109/ASRU57964.2023.10389733.

A USE OF LARGE LANGUAGE MODELS

This paper was written by the authors. Large language models (LLMs) were used only for minor language polishing.

B DETAILS OF TRAINING PROCEDURE

B.1 SIMULATION OF TRAINING DATASET

Clean speech source The model is trained with VCTK training set. VCTK corpus (Yamagishi et al., 2019) is a multi-speaker English corpus containing 110 speakers with different accents. We split it into a training part VCTK-Train and a testing part VCTK-Test. The version of VCTK we used is 0.92. To follow the data preparation strategy of previous restoration studies Liu et al. (2022b), only the *mic1* microphone data is used for experiments, and *p280* and *p315* are omitted for the technical issues. For the remaining 108 speakers, the last 8 speakers, *p360, p361, p362, p363, p364, p374, p376, s5* are split as test set VCTK-Test for super-resolution sub-task. Within the other 100 speakers, *p232* and *p257* are also excluded because they are used in the test set VCTK-ND and VCTK+DEMAND datasets. Therefore, the remaining 98 speakers are used as training data.

Simulation pipeline To simulate input signal for training, we randomly applied the various distortions based on the pipeline as shown in Figure 4. In particular, we sequentially applied physical and digital distortions. The physical distortions include convolution of transfer function mainly caused by reverberation at indoor environment. We used RIR samples from DNS dataset (Reddy et al., 2022). Note that we compensated time-delay effect from the convolution by applying direct component of RIR to the corresponding target speech signal. Then, as a second physical distortion, we added various background and interfering noises using noise samples (Reddy et al., 2022) and simulated colored gaussian noise. Each noise source is independently applied with signal-to-noise (SNR) ratio ranging from 0 to 20 dB. Then, as a final stage of physical distortion, we applied band pass filtering (BPF) to account for the recording condition of microphone such as occlusion, hardware properties, in this study, we mainly considered occlusion effect for the simulation. Also, to remove the phase distortion from the BPF, we applied as zero-phase filtering because the model does not need to consider these effect, only to make the learning process complicated. As a final step for physical simulation, we randomly scaled the level of signals from -35 to -15 dB Full Scale (dBFS). We also scaled the speech sources along with the corresponding input.

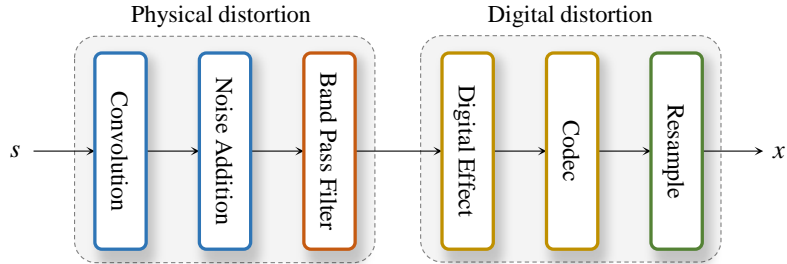


Figure 4: **Noisy-distorted speech input simulation pipeline.** The simulation procedure is partitioned to physical distortion and digital distortion.

Then, three kinds of digital distortions were simulated in sequence. We randomly applied audio clipping, crystalizer, flanger, and crusher as digital effects, each introducing characteristic non-linear saturation, spectral over-enhancement, comb filtering, or quantization noise (detailed parameter ranges are summarized in Table 5). Afterward, digital codec compression was applied to emulate transmission artifacts, using either MP3 or OGG (Vorbis/Opus) encoding. Finally, the processed signals were randomly downsampled to 8 or 16 kHz to simulate low-bandwidth recording and communication scenarios.

Table 5: List of applied distortions with probabilities and parameter ranges.

Augmentation	Prob.	Param. name	Range / Values	Notes
RIR convolution	0.50	-	-	direct-path delay compensated
Sample Noise	1.00	SNR (dB)	[0, 20]	from DNS dataset
Colored Gaussian Noise	1.00	SNR (dB)	[0, 20]	
		exponent β	[0.75, 1.5]	
Band-limiting (BPF) (occlusion FIR)	0.5	f_1 (Hz)	[500, 1500]	zero-phase
		f_2 (Hz)	$f_1 + [200, 500]$	transition band upper edge
		cut_gain	(0.1, 0.3)	stopband gain, applied as g^β
		β	[0.25, 1.00]	(thus effective stopband $\approx [0.22, 0.55]$)
		taps	odd in [31, 61]	<code>firwin2</code> , $f_s=16k$ ($f_N=8k$)
Clipping	0.5	level (dB)	[-15, 0]	hard clipping threshold
Crystallizer	0.15	intensity	[1, 4]	spectral “sharpening”
Flanger	0.05	depth	[1, 5]	short-delay comb filtering
Crusher (bit-depth)	0.10	bits	[1, 9]	quantization/aliasing
Codec (any)	0.30	—	—	one of the following
MP3		bit rate (kbps)	[4, 16]	variable bit-rate sampled uniformly
OGG		encoder	vorbis, opus	random choice
Frequency Masking	1.00	F_{bw} (freq. bins)	[0, 10]	
		# masks	[0, 3]	set to [0, 1] in adversarial training
Time Masking	1.00	T_{dur} (frames)	[0, 10]	
		# masks	[0, 2]	set to [0, 1] in adversarial training
Downsample	1.00	target f_s	{8k (0.25), 16k (0.75)}	

B.2 TRAINING DETAILS

For pretraining, TF-Restormer was optimized with batch size set to 2 to train on a single GPU of NVIDIA RTX 6000 Ada Generation 48GB and AdamW (Loshchilov & Hutter, 2019) as our optimizer. For pretraining, we update 200,000 steps with VCTK dataset. The length of training utterance is set to 3 seconds. Then, adversarial training is followed with 200,000 steps. For both the stages, we use learning rate 2.0e-4 with betas (0.9, 0.995) and learning rate decay 0.9 at every 10,000 steps after 100,000 steps for pretraining whereas 10,000 steps for adversarial training.

Each stage is trained with a linear warm-up for 5,000 steps for the generator. On the other hand, the discriminators in the adversarial training perform 2 optimizations for every single generator’s optimization step without warm-up. For the discriminators, the AdamW optimizer is used with betas (0.8, 0.999). Based on conventional multi-scale STFT discriminators (Défossez et al., 2023), we used the proposed multi-scale SFI-STFT discriminator with STFT window durations of [20, 40, 60, 80, 100] ms, which allows for the capture of spectral information at different resolutions.

C DETAILS OF MODEL CONFIGURATION

For TF-Restormer, C_E and B_E for encoder are set to 128 and 6 while C_D and B_D are set to 64 and 3. The kernel size in ConvFFN and the number of heads in MHSAs/MHCA are commonly set to $K = 7$ and $H = 4$, respectively. For frequency projection layer, F_{proj} is set to 512.

For offline TF-Restormer, each input mixture is normalized by dividing it by its standard deviation and the enhanced output is rescaled by the same factor. For streaming version of TF-Restormer, two mamba blocks are used in the time module with $d_{state} = 16$, causal Conv1D kernel size 3 with expansion factor 4. For streaming version, we still use the non-causal Conv2D layer for input and output projection for robust restoration, therefore the latency increases by two frames, total latency of 80ms (40 ms window, 20 ms hop). Overall, the model size of TF-Restormer is 30.1M for offline mode and 19.0M for streaming mode, which are smaller sizes compared to the existing models.

C.1 COMPARISON OF THE MODEL SIZE AND RTF

In Table 6, we compare model size and multiply-accumulate operations (MACs) for a 1-second-long input using *ptflops* package². We also measure real-time factor (RTF) measured on 4-second-long

²<https://github.com/sovrasov/flops-counter.pytorch>

Table 6: Comparison of the model size and RTF. RTF is calculated on NVIDIA RTX 4090. [†]We utilized pretrained models from open implementation code from UNIVERSE++ (Scheibler et al., 2024). [‡]The model size of FINALLY includes WavLM whose model size is 358M.

Model	Model Size (M)	$f_E \rightarrow f_D$ (kHz)	MACs(G)	RTF
VoiceFixer	70.3	44.1 → 44.1	12.9	0.010
StoRM	55.1	16 → 16	156.4	0.520
UNIVERSE [†]	46.4	16 → 16	36.9	0.014
UNIVERSE++ [†]	84.2	16 → 16	36.9	0.015
FINALLY [‡]	454.0	16 → 48	—	—
TF-Locoformer	14.9	16 → 16 48 → 48	246.9 731.6	0.025 0.088
TF-Restormer	30.1	8 → 16	240.8	0.009
		8 → 44.1	308.4	0.017
		16 → 16	440.9	0.034
		16 → 48	518.7	0.053
		8 → 16	114.7	0.012
TF-Restormer- <i>streaming</i>	19.0	8 → 44.1	138.1	0.018
		16 → 16	214.5	0.035
		16 → 48	242.0	0.049

samples with an NVIDIA RTX 4090. Conventional models operate at fixed input-output sampling rates, which results in fixed MACs regardless of the task configuration. In contrast, TF-Restormer adapts its computation depending on the input and output rates f_E and f_D .

Among baselines, StoRM requires 50 diffusion steps, leading to very high MACs and RTF despite its moderate model size. UNIVERSE and UNIVERSE++ reduce the number of steps (8 by default in the open implementation), which lowers the runtime cost compared to StoRM, but their model sizes remain relatively large and the diffusion process cannot be adapted for streaming, representing a fundamental limitation. TF-Locoformer, built on a dual-path design, involves higher computational complexity but benefits from effective parallelism, so its RTF is not as large as its MACs might suggest; its parameter size is also smaller than most diffusion- or vocoder-based systems.

Our proposed TF-Restormer also follows a dual-path formulation, so the raw MACs are relatively large. Nevertheless, RTF remains low in practice, comparable to or even faster than prior dual-path models. Crucially, TF-Restormer optimizes computation according to the input and output sampling rates: for instance, in the $8 \rightarrow 16$ kHz setting, redundant high-frequency processing is skipped, yielding a very low RTF. Also, the streaming variant maintains consistently low RTF while preserving accuracy, demonstrating its suitability for real-time applications.

D SIMULATION OF VCTK NOISY DISTORTED INPUT

The noisy-distorted input from VCTK testset in Table 3 was generated by corrupting clean VCTK utterances with additive noise from DEMAND (Thiemann et al., 2013) and colored Gaussian noise, RIR samples from RWCP (Nakamura et al., 2000) and AIR (Jeub et al., 2009) for reverberation, and distortions such as clipping and band-limiting. Additional digital effects including audio codecs (MP3, OGG) were applied before resampling to various rates (8-48 kHz). This simulation aligns the training pipeline while maintaining samples partitioning of speech, noise, and RIR sources.

The details of parameter range are summarized in Table 7.

E ABLATION DETAILS

E.1 EFFECTS OF SCALED LOG-SPECTRAL LOSS

Figure 5 illustrates the gradient behavior of the proposed scaled log-spectral loss, defined as $\partial\ell/\partial d = w/(d+w)$ where $d = |y - s|$ denotes the spectral distance and w is a scale factor. Unlike conventional ℓ_1 or ℓ_2 criteria, whose gradients are either constant regardless of error magnitude (ℓ_1) or increase proportionally with larger errors (ℓ_2), the proposed formulation yields gradients that are strongest near $d \approx 0$ and gradually diminish once d exceeds w . This mechanism emphasizes re-

Table 7: List of applied distortions with probabilities and parameter ranges.

Augmentation	Prob.	Param. name	Range / Values	Notes
RIR convolution	0.50	-	-	direct-path delay compensated
Sample Noise	1.00	SNR (dB)	[5, 20]	from DNS dataset
Colored Gaussian Noise	1.00	SNR (dB)	[5, 20]	
		exponent β	[0.75, 1.5]	
Band-limiting (BPF) (occlusion FIR)	0.20	f_1 (Hz)	[2000, 4000]	zero-phase
		f_2 (Hz)	$f_1 + [200, 500]$	transition band upper edge
		cut_gain	(0.1, 0.3)	stopband gain, applied as g^β
		β	[0.25, 0.75]	(thus effective stopband $\approx [0.22, 0.55]$)
		taps	odd in [31, 61]	<code>firwin2</code> , $f_s=16k$ ($f_N=8k$)
Clipping	0.20	level (dB)	[-10, 0]	hard clipping threshold
Crystalizer	0.10	intensity	[1, 2]	spectral “sharpening”
Flanger	0.05	depth	[1, 3]	short-delay comb filtering
Crusher (bit-depth)	0.10	bits	[1, 5]	quantization/aliasing
Codec (any)	0.25	—	—	one of the following
MP3		bit rate (kbps)	[16, 64]	variable bit-rate sampled uniformly
OGG		encoder	vorbis, opus	random choice
Frequency Masking	1.00	F_{bw} (freq. bins)	[0, 5]	
		# masks	[0, 1]	
Time Masking	1.00	T_{dur} (frames)	[0, 5]	
		# masks	[0, 1]	

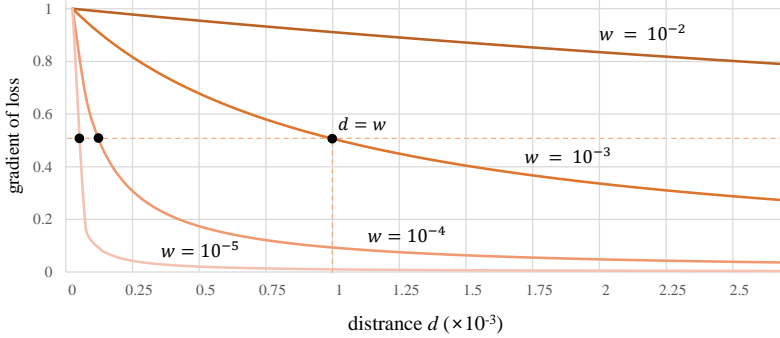


Figure 5: Gradient profiles of the proposed scaled log-spectral loss $\partial\ell/\partial d = w/(d + w)$ for different scale factors w . The curves show that the gradient is 1 near zero error and monotonically decreases as the distance $d = |y - s|$ grows. Smaller w values make the loss more sensitive to fine spectral deviations, while larger w values maintain stronger gradients over broader error ranges.

gions where the spectrum is already well-aligned, thereby preserving fine details, while suppressing unstable updates from heavily corrupted regions. The figure shows that when $d = w$, the gradient magnitude stabilizes at 0.5, providing a natural balance between emphasizing accurate components and de-emphasizing severely mismatched ones. As w decreases, the loss becomes more sensitive to smaller deviations, further suggesting subtle spectral structures that are otherwise neglected in conventional losses.

E.2 ILLUSTRATION OF ENCODER-DECODER STRUCTURE ABLATION

Figure 6 provides detailed comparisons of the three decoder designs considered in our ablation.

(a) Decoder-only. This variant directly inserts extension queries into the decoder without an encoder counterpart. The decoder therefore bears the full burden of modeling both the observed input band and the missing high-frequency bands, resulting in heavier computation and weaker inductive bias from the input.

(b) Encoder-decoder without MHCA. Here the encoder first analyzes the input bandwidth, and the decoder has the same internal structure as the encoder but receives projected extension queries.

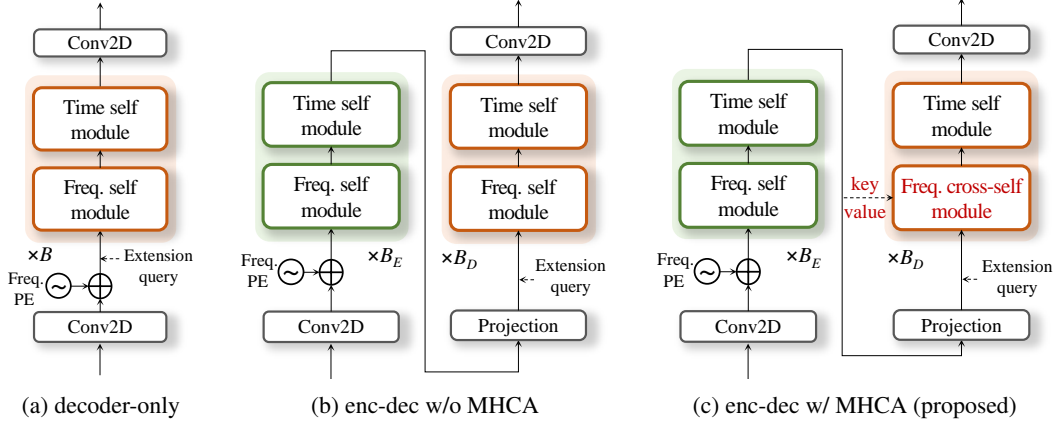


Figure 6: **Unit modules in TF-Encoder and TF-Decoder.** The (a) time module is based on MHSA with RoPE while (b) the frequency encoder module is based on MHSA with frequency projection layer. (c) The frequency decoder module utilize MHCA based on key/value from the encoder features

Although this design separates analysis and reconstruction, the decoder relies only on self-attention within the extended sequence, and does not explicitly exploit encoder features for reconstruction.

(c) Encoder-decoder with MHCA (proposed). In our final design, the decoder additionally uses a frequency cross-self module, where encoder outputs serve as key-value inputs for cross-attention while extension queries act as queries. This enables direct conditioning of high-frequency synthesis on encoder features, while the self-attention within the decoder refines spectral structure among extended bins. As a result, the encoder specializes in processing the observed input, and the lightweight decoder focuses on plausible high-frequency generation guided by encoder information.

These illustrations highlight how the proposed encoder-decoder with MHCA achieves a clear division of labor: the encoder concentrates on input-bandwidth analysis, and the decoder selectively extends spectral content with cross-conditioning, leading to better efficiency and stability compared to the other two designs.

F EVALUATION ON REAL-RECORDED DATASET

VoxCeleb Data We test TF-Restormer on 50 selected utterances from VoxCeleb1 (Nagrani et al., 2017), balanced across gender and covering the Speech Transmission Index (STI) range 0.75-0.99, to examine performance on real-recorded speech with diverse speakers (Su et al., 2020). For VoxCeleb Data, our TF-Restormer shows as natural restoration outputs as recent competing vocoder or diffusion-based methods in terms of UTMOS, WVMOS, and DNSMOS.

Table 8: Comparison with prior work on Voxceleb real data.

VoxCeleb (HiFi-GAN-2 validation set, real data)			
Model	UTMOS (\uparrow)	WVMOS (\uparrow)	DNSMOS (\uparrow)
Input	2.76 ± 0.13	2.90 ± 0.16	2.72 ± 0.11
HiFi++ (Andreev et al., 2022)	2.76 ± 0.13	2.68 ± 0.14	2.98 ± 0.07
VoiceFixer	2.60 ± 0.09	2.79 ± 0.09	3.08 ± 0.06
DEMUCS (Défossez et al., 2019)	3.51 ± 0.08	3.72 ± 0.08	3.27 ± 0.04
StoRM	3.29 ± 0.08	3.54 ± 0.09	3.17 ± 0.04
BBED (Lay et al., 2023)	3.30 ± 0.10	3.47 ± 0.08	3.23 ± 0.04
HiFi-GAN-2 (Su et al., 2021)	3.67 ± 0.09	3.96 ± 0.06	3.32 ± 0.03
FINALLY (Babaev et al., 2024)	4.05 ± 0.07	3.98 ± 0.06	3.31 ± 0.04
TF-Restormer	3.98 ± 0.09	3.82 ± 0.09	3.34 ± 0.06
TF-Restormer-streaming	3.64 ± 0.10	3.59 ± 0.12	3.29 ± 0.04

G LIMITATIONS AND FUTURE WORKS

Although TF-Restormer shows balanced improvements in signal fidelity and perceptual quality, several limitations remain. First, when the input speech is severely degraded, the high uncertainty in the observations can induce content or speaker artefacts. This reflects a common trade-off in speech restoration: adversarial training encourages perceptually natural reconstructions by sampling plausible high-frequency details, but can deviate from the exact clean reference, whereas purely supervised objectives stay closer to the ground truth yet tend to average out details, producing less natural-sounding results. Second, the model may exhibit language dependency. Because it is trained on extremely distorted scenarios with limited single-language datasets, the model (and WavLM used for perceptual loss) may amplify language-specific biases (e.g. memorizing certain phonetic patterns).

Finally, while the model targets universal speech restoration, it does not address multi-speaker scenarios such as separation or extraction. Future work includes mitigating artefacts under extreme degradations, extending training to multilingual and more diverse corpora, and adapting the framework to handle overlapped multi-speaker speech. Note that the TF dual-path architecture was originally proposed in speech separation, suggesting its potential extension to separation tasks.